Nanoscale Res Lett (2009) 4:955–961
DOI 10.1007/s11671-009-9324-8

NANO PERSPECTIVES

Field Emission Properties and Fabrication of CdS Nanotube Arrays

Xuemin Qian · Huibiao Liu · Yanbing Guo · Shiqun Zhu · Yinglin Song · Yuliang Li

Received: 23 February 2009 / Accepted: 14 April 2009 / Published online: 5 May 2009

Abstract A large area arrays (ca. 40 cm^2) of CdS nanotube on silicon wafer are successfully fabricated by the method of layer-by-layer deposition cycle. The wall thicknesses of CdS nanotubes are tuned by controlling the times of layer-by-layer deposition cycle. The field emission (FE) properties of CdS nanotube arrays are investigated for the first time. The arrays of CdS nanotube with thin wall exhibit better FE properties, a lower turn-on field, and a higher field enhancement factor than that of the arrays of CdS nanotube with thick wall, for which the ratio of length to the wall thickness of the CdS nanotubes have played an important role. With increasing the wall thickness of CdS nanotube, the enhancement factor β decreases and the values of turn-on field and threshold field increase.

X. Qian · S. Zhu · Y. Song (✉)
School of Physical Science and Technology, Suzhou University, Suzhou, Jiangsu Province 215006, People's Republic of China
e-mail: ylsong@hit.edu.cn

X. Qian
e-mail: qianxuemin1813@sina.com

S. Zhu
e-mail: szhu@suda.edu.cn

X. Qian · H. Liu (✉) · Y. Guo · Y. Li
Beijing National Laboratory for Molecular Sciences (BNLMS), CAS Key Laboratory of Organic Solid, Institute of Chemistry, Chinese Academy of Sciences, Beijing 100190, People's Republic of China
e-mail: liuhb@iccas.ac.cn

Y. Guo
e-mail: guoyb@iccas.ac.cn

Y. Li
e-mail: ylli@iccas.ac.cn

Keywords CdS · Nanotube arrays · Layer-by-layer deposition · Field emission

Introduction

One-dimensional semiconductor nanostructures have been intensively investigated in recent years due to their interesting optical and electronic properties, and promising applications in nanoscale devices [1–3]. Among the II–VI semiconductors, CdS has been attracted special interest because it exhibits high photosensitivity and its band gap energy (2.41 eV) appears in the visible spectrum leading to many commercial or potential applications in light-emitting diodes, solar cells, field emitter, and other photoelectric devices [4–8]. To date, CdS nanotubes are synthesized via the sol–gel or electrophoretic processing combination of molecular anchor template and various porous membranes including anodic aluminum oxide, polycarbonate, and mesoporous silica. [9–12] In fact, the CdS nanotubes prepared by above-mentioned methods are always free standing, and impossible to be directly used to fabricate nanodevices, because they cannot orderly locate on the solid surface after the removal of the templates. Therefore, the controlling growth of aligned CdS nanotubes and getting ordered nanostructures on conductive substrates by a facile and versatile synthetic method is still a challenge. In this work, a large area of CdS nanotube arrays on silicon wafer is successfully fabricated by the method of layer-by-layer deposition using well-aligned ZnO nanorod arrays as removable templates. The wall thicknesses of CdS nanotubes are precisely tuned by controlling the cycles of layer-by-layer deposition. The field emission (FE) properties of CdS nanotube arrays are investigated. The results indicate that the FE properties of CdS nanotube arrays can be

controlled through changing the wall thicknesses of CdS nanotubes. With increasing the wall thicknesses of CdS nanotubes, the enhancement factor β decreases and the values of turn-on field and threshold field increase.

Experimental Details

Scheme 1 shows a schematic illustration of the fabrication processes of CdS nanotube arrays by the method of layer-by-layer deposition. A typical synthetic procedure is carried out as follows. The ZnO nanorod arrays are prepared on a silicon wafer through a hydrothermal process [13]. Then, the wafer with ZnO nanorod arrays is immersed in an aqueous solution of 0.05 M cadmium nitrite. In this process, the Cd^{2+} nuclei will adhere to the lattice site on the surface of ZnO nanorods. After 5 min, the wafer is taken out from the solution and washed with deionized water for 3 times. Then, the wafer is dipped into an aqueous solution of 0.05 M sodium sulfide for 5 min resulting in the Cd^{2+} reacting with S^{2-} to form CdS nuclei on the surface of ZnO nanorod. Subsequently, the wafer is washed with deionized water for 3 times. Repeating the above-mentioned process for 3 times, the wafer becomes slightly yellow, which indicates the CdS layer on the surface of ZnO nanorods is formed. Three kinds of ZnO/CdS core/shell nanorod arrays with different thicknesses of CdS shell are prepared by above-mentioned process for 6 (sample C), 9 (sample B), and 12 (sample A) deposition cycles, respectively. Then, three samples are immersed in the aqueous solution of 1 M sodium hydroxide to remove the ZnO nanorods, respectively. After removing the ZnO nanorods, the wafers show the bright yellow of CdS nanotubes.

The arrays of CdS nanotubes are characterized and analyzed by field emission scanning electron microscopy (FESEM, Hitachi, S-4300), transmission electron microscopy (TEM, JEOL, JEM-1011), energy-dispersed X-ray microanalysis system (EDXA, Oxford Instrument, UK), Fluorescence spectrophotometer (Hitachi, F-4500), and X-ray diffraction (XRD). The XRD patterns are recorded with a Japan Rigaku D/max-2500 rotation anode X-ray diffractometer equipped with graphite-monochromatized Cu Kα radiation ($\lambda = 1.54178$ Å), employing a scanning rate of $0.05°s^{-1}$ in the 2θ range from 20° to 60°. The FE properties of CdS nanotube arrays are measured using a two-parallel-plate configuration in a homemade vacuum chamber at a base pressure of $\sim 1.0 \times 10^{-6}$ Pa at room temperature. The sample is attached to one of stainless-steel plates as cathode with the other plate as anode. The distance between the electrodes is 300 μm. A direct current

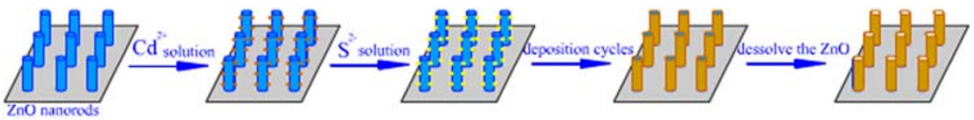

Scheme 1 The schematic illustration of the fabrication processes of CdS nanotube arrays

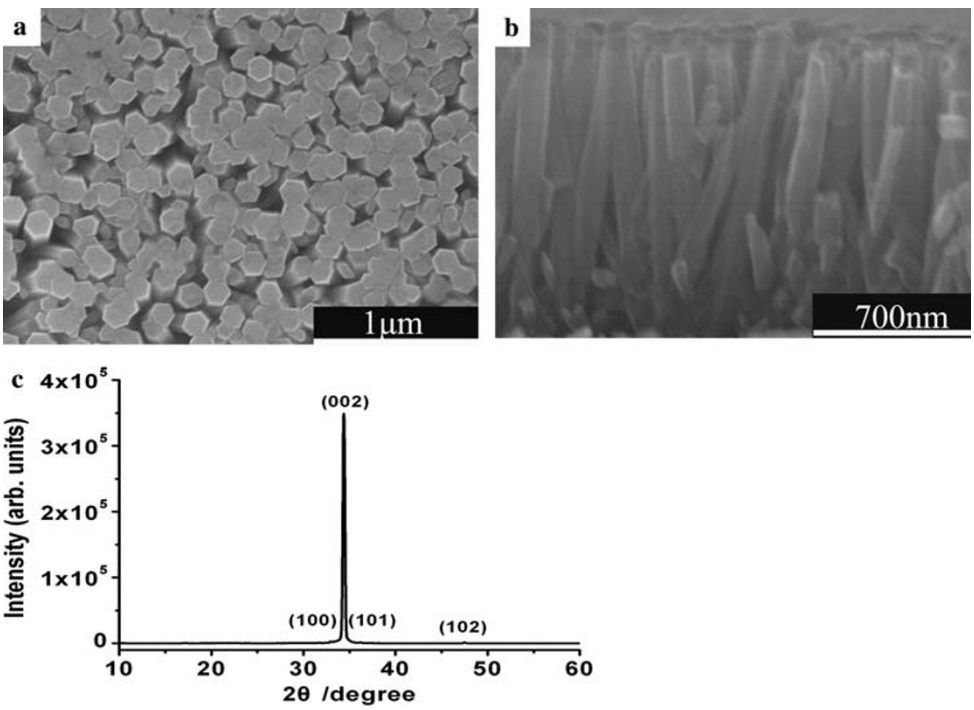

Fig. 1 SEM images of ZnO nanorod arrays **a** the top view, **b** the cross-sectional view. **c** The XRD pattern of ZnO nanorod arrays

voltage sweeping from 0 to 5000 V was applied to the sample at a step of 50 V. The emission current is monitored using a Keithley 6485 picoammeter.

Results and Discussion

The morphologies of pre-synthesized ZnO nanorod arrays are first examined by SEM. Figure 1a shows that the ZnO nanorods present a well-defined hexagonal shape with uniform diameter of about 126 nm. The cross-sectional view of SEM image (Fig. 1b) shows the ZnO nanorods align on the silicon wafer with a length of about 1.5 μm. Such highly alignment of ZnO nanorods are further confirmed by its corresponding XRD analysis. As shown in Fig. 1c, the XRD pattern is dominated by a very sharp and strong (002) reflection of wurtzite-type ZnO, which indicates the ZnO nanorods are grown in the preferentially direction of [0001]. After the 12 cycles of deposition CdS and subsequent ZnO nanorods template removal, the olivaceous film changes to light yellow and remains on the silicon wafer. Figure 2a shows that the photograph of large area light yellow CdS nanotube arrays (sample A), which are up to 40 cm^2 on size. Figure 2b displays that the XRD pattern of sample A which is dominated by characteristic (002), (102), and (110) reflections of wurtzite-type CdS, which indicates the crystal of as-synthesized CdS nanotube. The EDAX pattern (Fig. 2c) shows that there are just S and Cd elements in the nanotubes, which confirms that the ZnO nanorods are completely removed. The quantitative analysis of EDAX pattern indicates that the atomic ratio of Cd and S in the nanotubes is about 1:1. The room temperature photoluminescence (PL) measurement of the CdS nanotube arrays are shown in Fig. 2d. A green emission band around 550 nm and a red emission band around 750 nm [14] are observed. The PL intensities of CdS nanotube arrays enhance with increasing the deposition cycles. As shown in Fig. 2e and f, the SEM images reveal that the light yellow film deposited on the surface of silicon wafer consists of perfectly aligned hexagonal CdS nanotube arrays. The hexagonal CdS

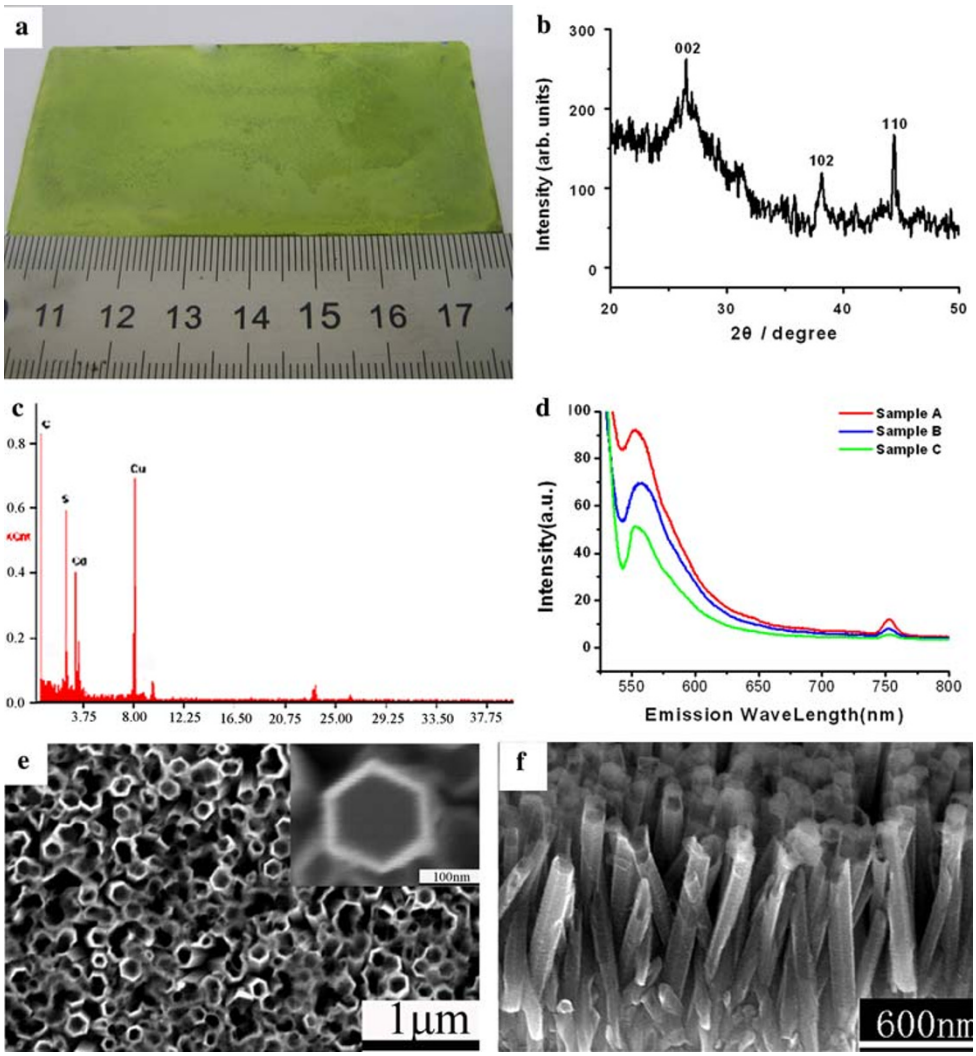

Fig. 2 **a** Photograph of sample A. **b** The XRD pattern of sample A. **c** The EDAX spectra of sample A. **d** PL spectrum of CdS nanotube arrays at room temperature, $\lambda_{ex} = 504$ nm. The SEM images of sample A **e** top view, **f** cross-section view

nanotubes resulting from the ZnO nanorod arrays have the average external diameters of 166 ± 7 nm (Fig. 2e), and all of nanotubes exhibit opened ends. The inset of Fig. 2e displays that their walls are very smooth about 20 ± 3 nm in thicknesses. Figure 2f shows the products present hollow structures vertically standing on the silicon wafer with a length of about 1.5 μm. When the deposition decreased to nine cycles, CdS nanotube arrays (sample B) are also obtained. Figure 3a shows that the average external diameters of CdS nanotubes are about 154 ± 5 nm, which are less than that of sample A (166 ± 7 nm). All of nanotubes exhibit opened ends in sample B. The wall thicknesses of CdS nanotubes (sample B) decrease to ca 15 ± 2.5 nm (Fig. 3b). With decreasing the deposition to six cycles, the arrays of CdS nanotube (sample C) with thinner wall thicknesses of 10 ± 1.5 nm are prepared, whose external diameters decrease to 140 ± 3 nm (Fig. 3d).

To explore construction forms of CdS nanotubes, the TEM measurements are performed. Figure 4a is a typical TEM image of CdS nanotube arrays (sample A). The nanotubes are uniform with an external diameter of about 166 nm and length of about 1.5 μm. Figure 4b shows a TEM image of typical individual CdS nanotube (sample A) with ca 166 nm of external diameter and the thickness of wall is about 20 nm. The selected area electron diffraction (SAED) pattern exhibits that the CdS nanotube (sample A) is polycrystal (the inset of Fig. 4b). As shown in Fig. 4c, the external diameters of CdS nanotubes (sample B) are about 154 nm and the open nanotube is clearly observed. The thicknesses of wall decrease to about 15 nm. The SAED pattern presents the CdS nanotube (sample B) also is polycrystal (the inset of Fig. 4c). Figure 4d shows that the external diameter of CdS nanotube (sample C) is about 140 nm and the thickness of wall is only about 10 nm. The inset of Fig. 4d indicates that the CdS nanotube (sample C) is polycrystal.

The FE measurements of CdS nanotube arrays dependence on wall thicknesses of nanotubes were firstly performed. The typical plot of the FE current density J versus the applied electric field (J–E) and the corresponding Fowler–Nordheim (F–N) plots of those CdS nanotube arrays are illustrated in Fig. 5a and b, respectively. The FE parameters are listed in Table 1. Here we define the turn-on field (E_{to}) and the threshold field (E_{th}) as the applied electric fields required to produce a current of 10 μA/cm^2 and 1 mA/cm^2, respectively. E_{to} for sample A is 11.33 V/μm. With decreasing the wall thicknesses of CdS nanotubes, the E_{to} of samples B and C decrease to 9.99 and 7.99 V/μm, respectively. With decreasing the wall thicknesses of CdS nanotubes, the E_{th} decreases. E_{th} for samples A, B, and C are 14.92, 13.44, and 11.27 V/μm, respectively. The maximum emission density of sample A is 3.9 mA/cm^2, which is higher than that of sample B (3.28 mA/cm^2) and C (2.97 mA/cm^2).

To further analyze the FE properties of the CdS nanotube arrays, the class Fowler–Nordheim (F–N) law [15],

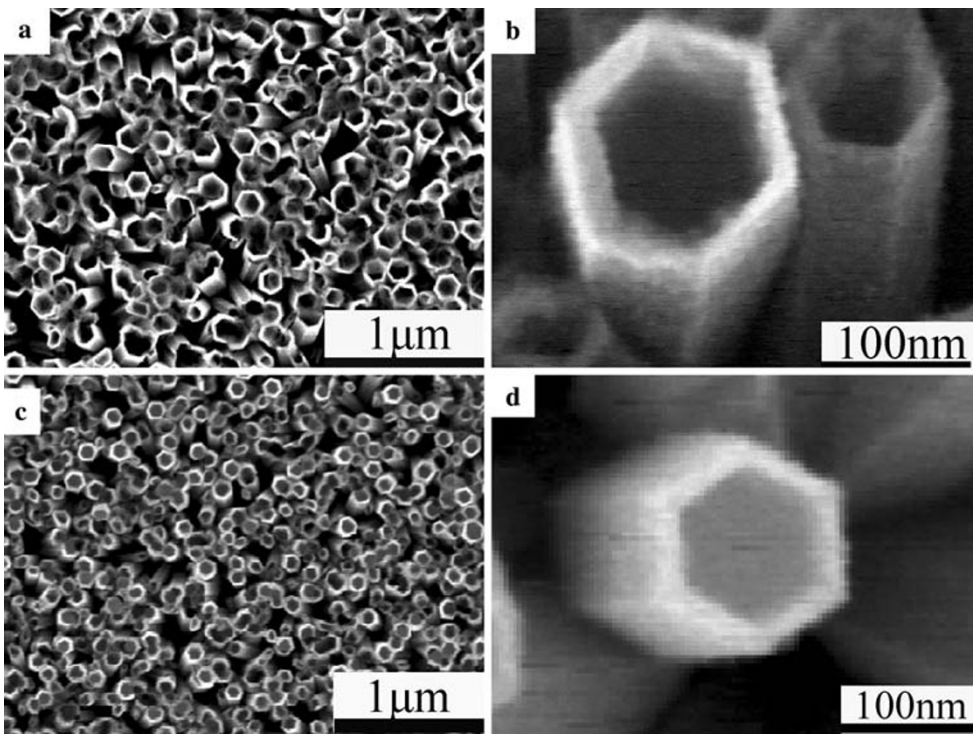

Fig. 3 SEM images of CdS nanotube arrays. **a** The low magnification SEM image of sample B. **b** The high magnification SEM image of sample B. **c** The low magnification SEM image of sample C. **d** The high magnification SEM image of sample C

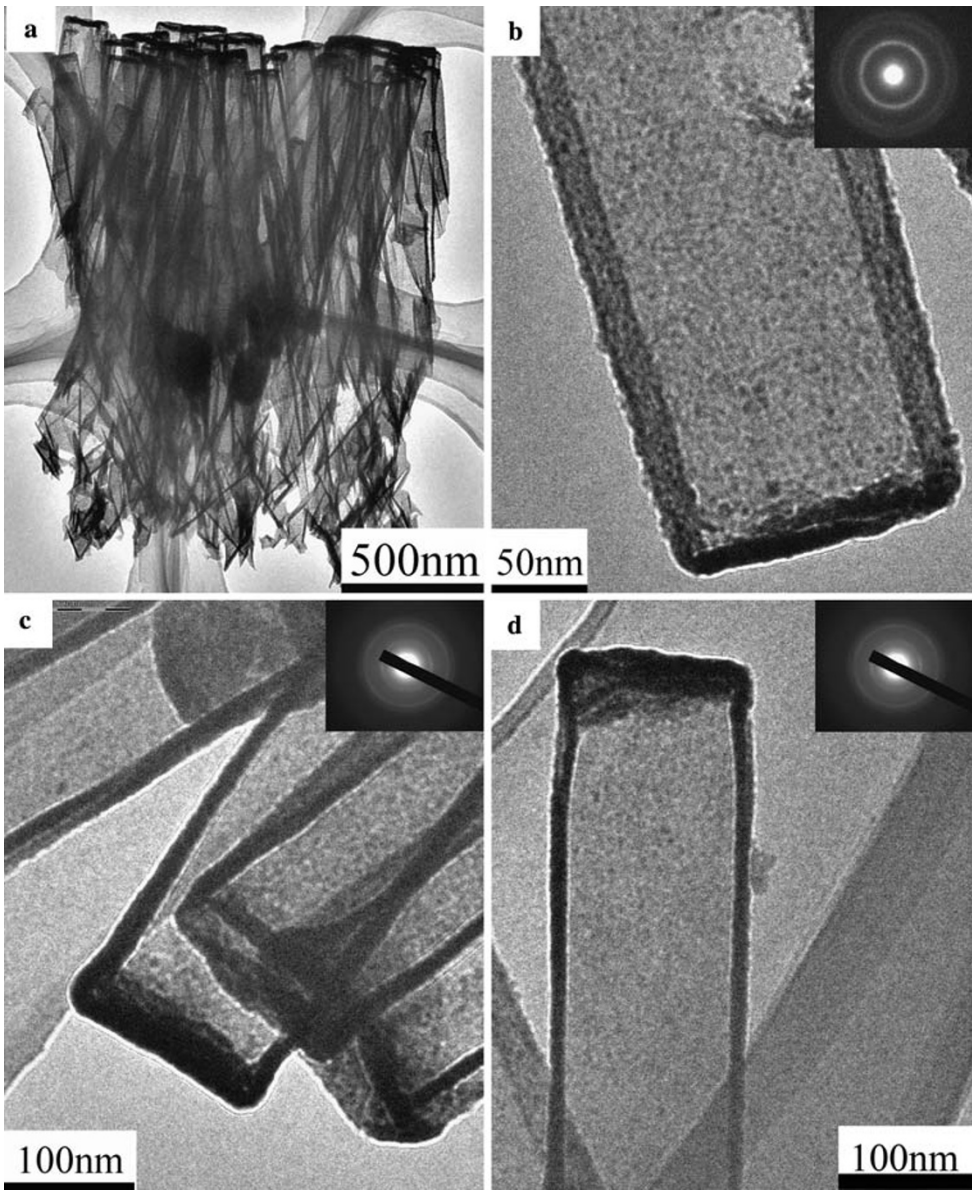

Fig. 4 **a** The low magnification TEM image of CdS nanotube arrays of sample A. TEM images of **b**, **c**, and **d** are high magnification TEM images of A, B, and C, respectively. The inset images are SAED patterns of corresponding CdS nanotube

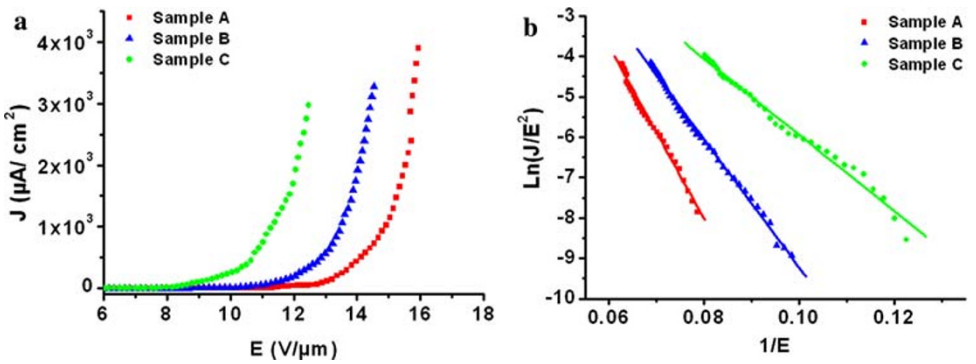

Fig. 5 **a** Field emission *J–E* curve of CdS nanotube arrays. **b** The corresponding F–N plot of CdS nanotube arrays

Table 1 The field emission properties of CdS nanotube arrays

Sample	*l*/*t*	*l*/*r*	E_{to} (V/μm)	E_{th} (V/μm)	β_{exp}	β_{sim}
A	75	18	11.33	14.92	276	273
B	100	19.5	9.99	13.44	372	359
C	150	21.4	7.99	11.72	625	642

r the average radius, *t* the thickness wall of CdS nanotube, *l* the length of nanotube, β_{exp} the value of enhancement factor obtained by experiment data, β_{sim} the simulation value of enhancement factor

which was induced on the base of the electron emission properties from a semi-infinite flat metallic surface, was used to describe the relationship between the J and the local field E_{local} nearby the emitter which is usually related to the average applied field E as follows:

$$E_{local} = \beta E = \beta \frac{V}{d} \quad (1)$$

where d is the inter-electrode spacing, V is the applied voltage, and β is the enhance factor. The F–N law is expressed as:

$$J = a\frac{\beta^2 E^2}{\phi}\exp\left(\frac{-b\phi^{3/2}}{\beta E}\right) \quad (2)$$

where $a = 1.54 \times 10^{-6}\,\mathrm{AV}^{-2}$, $b = 6.83 \times 10^{9}\,\mathrm{Vm}^{-1}\mathrm{eV}^{-3/2}$, and ϕ is the work function, which is estimated as 4.2 eV for CdS [16]. The β can be determined by fitting the slope value and taking a reasonable value. For those CdS nanotube arrays, the F–N plots (Fig. 5b) show a linear relationship, implying that a quantum-tunneling mechanism is responsible for the emission. As illustrated in Table 1, the β for sample C (625) is higher than that of samples A (276) and B (372). It is well-known that the β is not only determined by the aspect ratio but also by the ratio of length to the wall thickness for the tube-like emitters [17, 18]. An empirical formula is obtained according to Kokkorakis' model: [17, 18]

$$\beta = m * \frac{l}{r} + n * \frac{l}{t} + c \quad (3)$$

where m, n, and c are alterable parameters. The r is the average radius of nanotube, l is the length of nanotube, and t is the thickness of wall. The β is determined by two factors, aspect ratio *l*/*r* and the ratio of length to wall thickness *l*/*t*. For getting the values of three parameters, we must use formula 3 to fit the values of β which are obtained in experiment. The parameters m, n, and c are obtained as 0.9, 3.7, and 6, for the best fit to the experimental datum. Using these parameters, we get three simulating values of β_{sim} for samples A, B, and C, which are 273, 359, and 642, respectively. They are consistent with the experiment values. In our case, *l*/*r* of those CdS nanotube arrays are almost same and the value of parameter n is larger than parameter m, which means *l*/*t* is the key role to determine the FE properties of CdS nanotube arrays. The FE properties of CdS nanotube arrays increase with the increase of *l*/*t*. The length of samples A, B, and C are almost same, so the arrays of CdS nanotube with the thinner wall exhibit the better FE property.

Conclusions

A large area of CdS nanotube arrays is fabricated by a facile way of layer-by-layer deposition. The wall thicknesses of nanotubes are controlled by tuning the deposition cycles. The FE properties of CdS nanotube arrays dependence on wall thicknesses are investigated and show infusive and regular results. With decreasing the wall thicknesses of CdS nanotubes, the value of E_{to} and E_{th} decrease and β increases. The thinnest walls of CdS nanotubes exhibit the least value of E_{to} and E_{th} for promising candidate materials on field emitters and nanodevices.

Acknowledgments This work was supported by the National Nature Science Foundation of China (20531060, 20473102, and 20571078) and the National Basic Research 973 Program of China.

References

1. J.S. Jie, W.J. Zhang, Y. Jiang, X.M. Meng, Y.Q. Li, S.T. Lee, Nano. Lett. **6**, 1887 (2006). doi:10.1021/nl060867g
2. A.M. Morales, C.M. Lieber, Science **279**, 208 (1998). doi:10.1126/science.279.5348.208
3. X.F. Duan, Y. Huang, R. Agarwal, C.M. Lieber, Nature **21**, 6920 (2003)
4. O. Hayden, A.B. Greytak, D.C. Bell, Adv. Mater. **17**, 701 (2005). doi:10.1002/adma.200401235
5. I. Visoly-Fisher, S.R. Cohen, D. Cahen, C.S. Ferekides, Appl. Phys. Lett. **83**, 4924 (2003). doi:10.1063/1.1632532
6. N. Kouklin, L. Menon, A.Z. Wong, D.W. Thompson, J.A. Woollam, P.F. Williams, S. Bandyopadhyay, Appl. Phys. Lett. **79**, 4423 (2001). doi:10.1063/1.1427156
7. Y.F. Lin, Y.J. Hsu, S.Y. Lu, S.C. Kung, Chem. Commun. **22**, 2391 (2006). doi:10.1039/b604309g
8. Z.H. Yin, Y.Z. Long, C.Z. Gu, M.X. Wan, J.L. Duvail, Nanoscale Res. Lett. **4**, 63 (2009). doi:10.1007/s11671-008-9203-8
9. C.N.R. Rao, A. Govindaraj, F.L. Deepak, N.A. Gunari, Appl. Phys. Lett. **78**, 1853 (2001). doi:10.1063/1.1359145
10. T.Y. Peng, H.P. Yang, K. Dai, X. Pu, K. Hirao, Chem. Phys. Lett. **379**, 432 (2003). doi:10.1016/j.cplett.2003.08.059
11. X.P. Shen, A.H. Yuan, F. Wang, J.M. Hong, Z. Xu, Solid State Commun. **133**, 19 (2005). doi:10.1016/j.ssc.2004.09.053
12. S.M. Zhou, Y.S. Feng, L.D. Zhang, Eur. J. Inorg. Chem. 1794 (2003). doi:10.1002/ejic.200200593
13. L. Vayssieres, Adv. Mater. **15**, 464 (2003). doi:10.1002/adma.200390108
14. H.B. Liu, Y.L. Li, H.Y. Luo, H.J. Fang, H.M. Li, S.Q. Xiao, Z.Q. Shi, S.X. Xiao, D.B. Zhu, Eur. Phys. J. D **24**, 405 (2003). doi:10.1140/epjd/e2003-00188-3

15. R.H. Fowler, L.W. Nordheim, Proc. R. Soc. Lond. A **119**, 173 (1928). doi:10.1098/rspa.1928.0091
16. J.B. Cui, K.B. Teo, J.T.H. Tsai, J. Robertson, W. Milne, Appl. Phys. Lett. **77**, 1831 (2000). doi:10.1063/1.1310628
17. G.C. Kokkorakis, A. Modinos, J.P. Xanthakis, J. Appl. Phys. **91**, 4580 (2002). doi:10.1063/1.1448403
18. G.C. Kokkorakis, J.A. Roumeliotis, J.P. Xanthakis, J. Appl. Phys. **95**, 1468 (2004). doi:10.1063/1.1638617